Northumbria Research Link

www.northumbria.ac.uk/nrl

northumbria
UNIVERSITY NEWCASTLE

Drag Reduction in Supersonic Blunt Bodies Using Opposing Jet and Nozzle Geometric Variations

Atiqa Bibi[a], Adnan Maqsood[a*] ,Salma Sherbaz[a] and Laurent Dala[b]

[a] *Research Centre for Modeling & Simulation, National University of Sciences and Technology, H-12 Campus, Islamabad, Pakistan*

[b] *Department of Mechanical & Construction Engineering, Northumbria University, Newcastle, United Kingdom*

Abstract

Passive and active flow control methods are used to manipulate flow fields to reduce acoustic signature, aerodynamic drag and heating experienced by blunt bodies flying at supersonic and hypersonic speeds. This paper investigate the use of active opposing jet concept in combination with geometric variations of the opposing jet nozzle to alleviate high wave drag formation. A numerical study is conducted to observe the effects of simple jet as well as jet emanating from a divergent nozzle located at the nose of a blunt hemispherical body. An initial discussion is presented of the complex shock wave pattern flow physics occurring when opposing jet ejected from a nozzle under various operating conditions interacts with the free stream flow. The complex flow physics that include long penetration and short penetration mode is studied in conjunction with effect on drag. The numerical setup consists of supersonic free stream flow interacting with an opposing sonic jet under varying pressure ratios. Initial computational results are validated by identifying prominent flow features as well as comparing available experimental data of surface pressure distributions. Preliminary validation is followed by the introduction of a divergent nozzle in the blunt body nose region. A series of numerical iterations are performed by varying nozzle geometric parameters that include nozzle divergent angle and nozzle length for a certain jet pressure ratio. Long penetration mode, short penetration mode as well as flow separations are captured accurately during the analysis. The results show a considerable reduction in drag by the use of a divergent nozzle. Specifically, 46 % and 56% reduction in drag coefficient is achieved at pressure ratio of 0.6 and 0.8 respectively in the divergent nozzle cases as compared to the simple blunt body without any nozzle.

Keywords: Blunt Body; Opposing Jet; Short Period Mode; Long Period Mode; Supersonic Drag Reduction

---

Nomenclature

L	=	Length of Divergent nozzle
θ	=	Angle of divergent nozzle
M_∞	=	Free Stream Mach number
M_J	=	Jet Mach number
$P_{O\infty}$	=	Free Stream Stagnation Pressure
P_{OJ}	=	Jet Stagnation Pressure
PR	=	Pressure ratio
P_∞	=	Free Stream Static Pressure
P_e	=	Nozzle Exit Pressure
d_J	=	Diameter of Jet
SPM	=	Short Penetration Mode
LPM	=	Long Penetration Mode

---

[*] Corresponding author.
  E-mail address: adnan@rcms.nust.edu.pk

1. Introduction

Although blunt profiles in high speed help in reducing heat transfer to the body, they also increase overall drag experienced by the body. This high value of drag can be useful in re-entry applications where it actually helps to reduce the velocity during re-entry. However, for supersonic transport applications, where greater velocities are advantageous, the blunt body profile produces unnecessary drag. Efforts to reduce drag have been under study since the very inception of high speed vehicles. In this regard the opposing jet concept has gained the most interest in the research community due to its reusability and relatively economic implementation as compared to other methods. Series of research efforts over the years have showed a marked decrease in both heat and drag experienced by blunt profiles using an opposing jet issuing from the fore body region. All applications whether supersonic, hypersonic can achieve more efficient flight missions by the use of counter flowing forebody jets. The high speed application band encompasses fighter jets, transport jets, reconnaissance systems, supersonic cruise missiles and Inter Continental Ballistic Missiles. Advancement in the study of the active flow control system can prove to be quite helpful in progressing research activities for the new space technologies such as Reusable Launch Vehicles, Orbital transfer vehicles, and the more commercial application of space tourism. The opposing jet can play a key role in overcoming the challenges of the severe flight conditions experienced in these rapidly advancing technologies.

1.1. Related Work

By the end of World War II supersonic flight gained great importance in the form of high speed rockets. The development of Inter-Continental Ballistic Missiles (ICBM) started in 1953[1]. From here began an era of supersonic vehicles which through further advancement have evolved into hypersonic travelers including jet aircrafts, missiles, space shuttles and re-entry vehicles. All these missions must combat a common feature of high drag, high temperature environment and high acoustic signature. Therefore, with the development of supersonic travelers in the early 1950's; efforts to combat their severe aerodynamic environments were also initiated alongside.

Studies on the use of opposing jet to manipulate flow fields began since early 1950's [2] . Early research in the area was concerned mainly on understanding flow physics of the opposing jet phenomena [3, 4] . The earliest work on heat transfer effects was made by Inouye[5] in which it was concluded that at low flow rates heat transfer to body decreases by the use of opposing jet. A similar conclusion was made by Warren [6] where nitrogen and helium gases were used as opposing jets. It was inferred that as long as the jet flow remains small enough to not penetrate the free stream, heat reduction over body will occur. However, Finley [7] pointed out that Warren's study included very low pressure ratios. Hence, larger pressure ratios beyond the unstable region actually help to reduce heating. This conclusion was also made in the work of Rashis [8].

In 1960s and 1970s, attention was directed towards the heat and drag reduction effects of opposing jets. Advancement in the research of opposing jet technology lead to the study of various other aspects such as effect of different jet ejection materials, effect of flow variation and geometric parameters. Warren [6] studied the effect of nitrogen and helium gas on heat transfer rates. Barber [9] studied the effects of hydrogen, helium and nitrogen jets and found the results to significantly vary with jet mass flow rates. From research it has been concluded that the flow field of an opposing jet from a blunt body in supersonic flow mainly depends upon factors such as jet to body diameter ratio, jet to free stream pressure ratio, jet and free stream mach numbers. Initially, Finley [7] studied effect of jet mach no, effect of jet to body diameter ratios, and pressure ratios. Riggins [10] studied the effect of varying exit Mach number and exit diameter of jet. His results showed a decrease in drag with decrease in exit Mach number and increase in jet exit diameter.

Hayashi [11, 12] experimentally and numerically studied the effect of change in jet exit diameter, temperature, mach number and pressure ratio. He found a decrease in heat loads with increase in pressure ratio, Daso et al. [2] carried out extensive experimental tests on jet ejection from the nose of blunt reentry body. Effect of changing angle of attack on heat and drag reduction was also catered. In his study, he varied alpha to 9˚ and found that in this range of alpha variation there was not much significant change in flow as compared to alpha 0˚ case.

Efforts to understand the opposing jet flow phenomena have leaded many researchers to identify specific regions of flow [2, 13-15]. Jarvinen and Adams [13] studied different jet penetration modes namely Long Penetration Mode (LPM) and Short Penetration Mode (SPM). They found that LPM occurred at low thrust rates whereas SPM occurred at high thrust rates. Moreover transition from LPM to SPM occurred at a fixed pressure ratio called as the 'critical pressure ratio'. A similar discussion can be found in the works of Hayashi and Zheng [14, 15]. Three different regions were identified based on pressure ratio. At small pressure ratios oscillation of shockwave may occur. The shockwave is dispersed and may have long standoff distances from the body. Flow may exhibit diamond shaped patterns. This is known as unstable region. At higher pressure ratios no oscillations

of shockwave occur and shock stand-off distances are lesser. A distinct bow shock and terminal shock can be observed. There exists a free stagnation point at which both the flows come to rest, and the jet flow reverses its direction towards the body creating a recirculation region. This is known as stable region. There also exists a transition region during which flow changes from unstable to stable region. This region is difficult to capture.

Alongside experimental work, many efforts are also being carried out to numerically simulate the opposing jet phenomena computationally [11, 16, 17] . Hayashi [11] not only validated results with experimentations but also carried out a series of iterations varying jet exit mach number and temperatures to gain results which would otherwise be difficult and time consuming to obtain through experiments. Through his study he showed that decrease in jet temperature decreases the heat flux. Nair et al. [16] validated numerical code by applying it to a number of different configurations of opposing jet. Bilal [17] numerically captured the shock standoff distance and also studied the transition mode from LPM to SPM.

Different jet ejection schemes have also been considered. Multiple jet ejection as opposed to single jet emanating from nose of body is one of the earliest concepts considered. One of the most initial experimental works done in this regard is that of Jarvinen [18]. It is an extensive report studying different configurations, jet nozzles, mach numbers as well as effect of angle of attack. The multiple jet scheme is very promising not only for heat reduction but also finds its application in Retro propulsion phenomenon for re-entry phase of space modules. There is however limited literature of this concept due to its difficulty in implementation experimentally, and high computational cost numerically. Cordell [19] studied numerically the works of Jarvinen [18]. Sriram [20] carried out experimental work on multiple micro jets.

 One of the most recent advancements in active flow control technologies is the use of combinational strategies. In these methods, the jet is combined with other techniques such as forward cavities or aero spikes to achieve better control over flow. The works of Tamada [21] show very promising results. He showed that by the use of jet-spike combination i.e. ejection of jet from an aero spike; better drag reduction can be achieved at much lower pressure ratios. His results show that the use of an aero spike reduces drag coefficient to almost half of the baseline case of Ogive body with no jet. Morimoto [22] also studied the jet-spike configuration and found a considerable reduction in heat flux.

Another combination strategy is the use of forward facing jet cavity [23, 24] . According to the works of Lu Haibo [23], the addition of a cavity in the flow path allows the jet to develop properly and aids to reduce initial instabilities experienced during jet free stream interaction. The present study is inspired by the jet combination strategy concept. It is suggested to use a divergent nozzle for jet ejection. The free stream conditions will remain constant. The jet pressure will be varied. Through a vast series of numerical simulations, an optimal nozzle configuration will be proposed that will provide better drag reduction at a lower pressure ratio.

2. General Flow Features

In order to gain a better understanding of the current CFD analysis, a detailed theoretical discussion is presented. It explains the various flow field structures obtained when jet ejected from nozzles of varying operating conditions interact with the free stream. Nozzles generally have three different operating conditions namely Over-expanded, Under-expanded and Highly Under-expanded. These conditions are dictated by the difference in free stream static pressure (P_∞) as well as nozzle exit static pressure (P_e). The literature to follow discusses each operating condition of nozzle as well as the flow field structures that can be expected when a jet ejected from such a nozzle interacts with the opposing free stream.

2.1.   Interaction of Over-Expanded Jet with Opposing Free Stream:

If nozzle exit pressure is less than ambient pressure ($P_e < P_\infty$) then flow is said to be Over-Expanded. The jet collapses towards the central axis through a series of shock waves in order to increase the pressure to ambient pressure at nozzle exit (

Fig. 1a). Flow separation occurs inside the nozzle. When such a jet interacts with free stream opposing flow, an increase in flow separation inside the nozzle is observed (

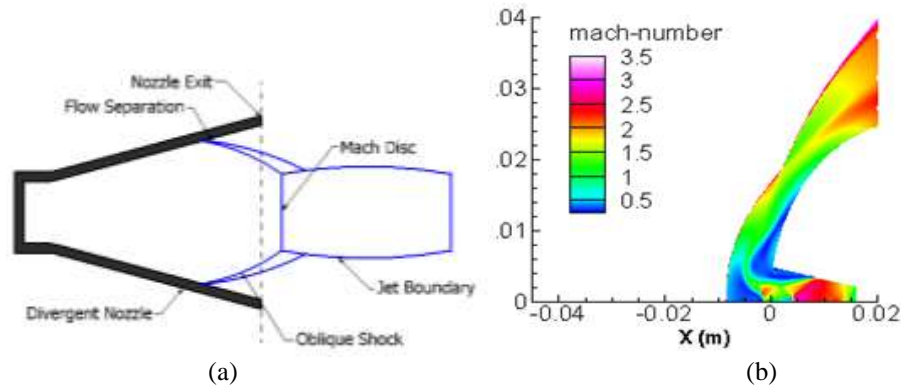Fig. 1b). This is a highly turbulent and undesirable phenomenon.

Fig. 1   Flow Conditions for Over Expanded Nozzle [25]

2.2.   Interaction of Slightly Under-Expanded Jet with Opposing Free Stream

If the nozzles exit pressure is slightly greater (1-2 times greater) than ambient pressure ($P_e > P_\infty$) the nozzle is said to be under-expanded. Weak expansion waves reflected from the jet boundary form compression waves. A series of compression and expansion waves form a diamond shaped pattern in the flow until ambient pressure is reached (fig. 2).
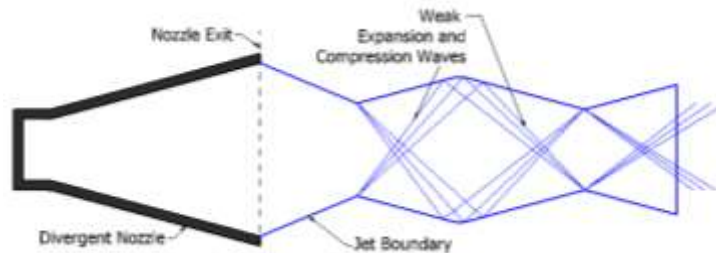

Fig. 2   Flow Conditions for Under Expanded Nozzle[26]

The diamond shaped pattern of and under-expanded jet can rupture the bow shock wave ahead of a blunt body in supersonic opposing flow. This causes the occurrence of the long penetration mode. Fig shows both schematic and experimental images of LPM mode as well as an image of LPM mode captured from current numerical analysis. This is also an undesirable unstable mode in which the shockwave is either diffused or oscillates axially. This mode is difficult to simulate numerically as it requires unsteady transient 3-d simulations to fully capture shock oscillations and there subsequent pitching effect imparted on blunt body.
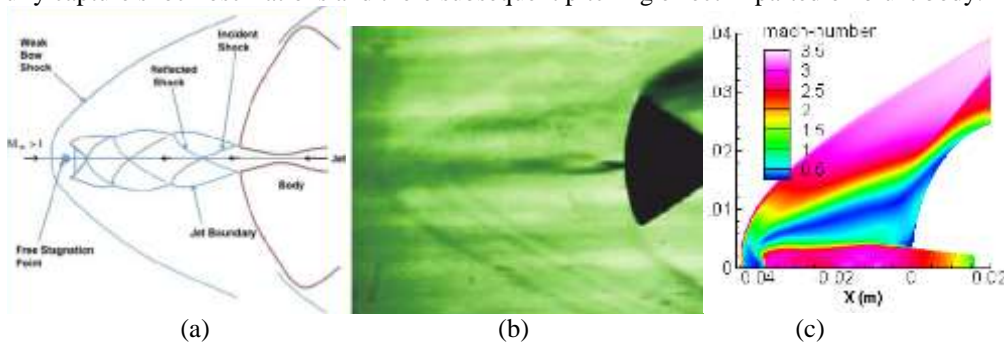

Fig. 3   Flow conditions for LPM (a) Schematic [15] (b) Experimental [2] (c) Computational

2.3.   Interaction of Highly Under-Expanded Jet with Opposing Free Stream

If the nozzle exit pressure is much greater than free stream ambient pressure (4 to 5 times greater) then the nozzle is said to be highly under expanded ($P_e \gg P_\infty$). The jet plume structure is terminated by a strong normal shockwave called as Mach Disc. Fig shows some of the distinct flow features which can be observed in this mode. The jet exiting from nozzle undergoes expansion until the jet pressure equals the ambient pressure,

4

thus forming a constant pressure jet boundary. Jet is reflected from jet boundary in the form of weak compression waves collectively forming a barrel shock. The rapid expansion in the jet core reduces the axial pressure to a limiting value at which a strong normal shock wave occurs. This is referred to as a mach disc or terminating shock. Flow upstream of the normal shock is highly supersonic whereas downstream flow is sub sonic. Flow beyond the barrel (oblique) shock is also supersonic but at lesser value then supersonic jet core. At the intersection point of barrel shock and mach disc a reflected shock emanates due to which this region is called as triple point. Jet flow passing through the reflected shock remains supersonic whereas flow passing through mach disc becomes subsonic. A slip line is defined in flow separating the external supersonic flow from inner subsonic jet core.
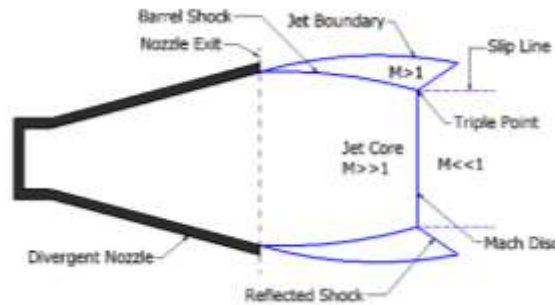

Fig. 4   Flow Conditions for Highly Under Expanded Nozzle [19]

A highly under expanded jet interacting with opposing free stream flow is desirable as it leads to the formation of the stable short penetration mode. Free stream supersonic flow ahead of blunt body is decelerated to subsonic by the bow shock wave. The supersonic jet flow is decelerated to subsonic by the mach disc. The two subsonic flows interact at the stagnation point. A contact surface arises from the stagnation point separating the subsonic free stream and jet flows. The interaction of free stream and jet flow produces a recirculation region over the body. This recirculation region emanates at the intersection point of terminating and barrel shock and stagnates on coming in contact with body. This recirculation region moves radially outwards with the increase in jet pressure. At a certain jet pressure the recirculation region completely clears the fore body and reattaches downstream forming a layer of protective fluid in the fore body vicinity, protecting it from high pressure and temperature loads.

The mode of penetration with distinct flow features described in literature above is called the blunt penetration mode. This is a desirable mode in which the flow remains stable and the shock wave is not bifurcated. The jet increases shock stand-off distance and its recirculation forms a protective layer over the body. This phenomenon has been found to significantly reduce fore body heat and drag loads. Fig shows both schematic and experimental images of SPM mode as well as an image of SPM mode captured from current numerical analysis.
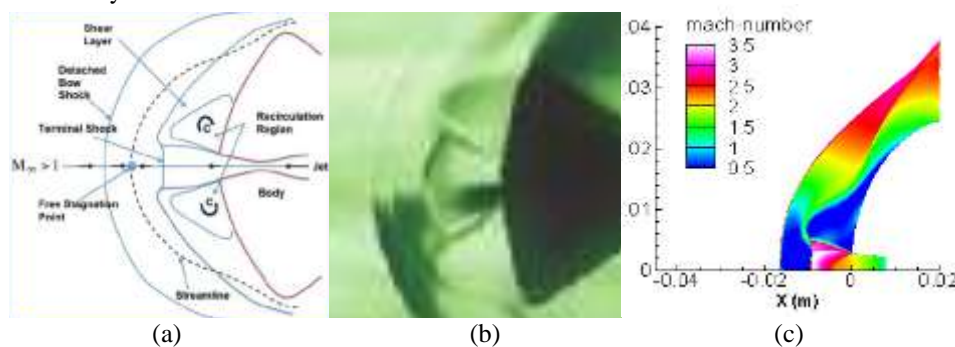

(a)   (b)   (c)

Fig. 5   Flow conditions for SPM (a) Schematic [15] (b) Experimental [2] (c) Computational

2.4.   Summary of Nozzle Theory

The three nozzle operating conditions depending upon nozzle exit pressures have been discussed in the literature above. Fig 6 is a pictorial summary of all three cases. It shows the flow conditions which occur when a nozzle under a certain operating condition interacts with an opposing flow. If a nozzle is over expanded ($P_e < P_\infty$) then opposing flow will cause flow separation (fig. 6a). If the nozzle is slightly under expanded ($P_e > P_\infty$) then opposing flow will cause the unstable long penetration mode (fig. 6b). If the nozzle is highly under

expanded ($P_e \gg P_\infty$), then opposing flow will produce the stable short penetration mode (fig. 6c). In the current analysis, the series of flow as well as nozzle geometric variations lead to the occurrence of one of these respective phenomena. The three images of fig 6 are therefore very important. Clear understanding of these images allows one to comprehend the operating condition of the nozzle as well as the subsequent flow mode produced when interacting with an opposing flow.
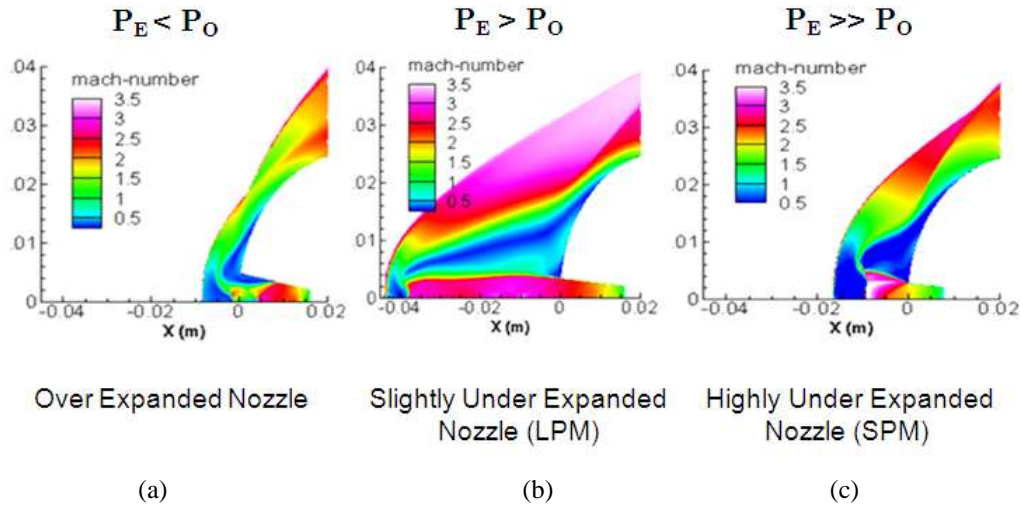

Fig. 6   Summary of Nozzle operating Conditions

3. Problem Description and Numerical Modeling

The basic aim of the current numerical analysis was to determine the drag reduction achieved by the simple opposing jet as well as opposing jet ejected from various divergent nozzle schemes. The baseline configuration with available experimental data is the hemispherical blunt body in supersonic flow, selected from the works of Hayashi et al. [27]. The flow conditions are similar to those used in the experimental works of Hayashi [27] summarized in **Error! Reference source not found.**.

	Gas	Air
Free Stream	Mach No.	**3.98**
	Stagnation Pressure (MPa)	**1.37**
	Stagnation Temperature (K)	**397**
	Gas	Air
Opposing Jet	Mach No.	**1**
	Stagnation Pressure Ratio (MPa)	**0.4, 0.6, 0.8**
	Temperature (K)	**300**
Wall	Temperature (K)	**295**

Table 1. Flow Conditions

3.1.   Problem Description

In the current study, initially, a numerical simulation of the simple hemispherical body without any jet was conducted. The hemispherical body was 50 mm in diameter as shown in **Error! Reference source not found.**. Grid independence study was also carried out. The surface pressure data were duly validated with experimental results. Numerical simulations were also computed to validate opposing jet cases. The jet ejection diameter was kept constant at 4 mm as shown in **Error! Reference source not found.**. The free stream conditions were also kept constant. However the jet Pressure Ratio (PR) was varied. PR is defined as 'the ratio of jet total pressure to free stream total pressure' (eq. 1). Flow analysis was conducted at three different pressure ratios of P.R = 0.4, 0.6 and 0.8. Surface pressure data was duly validated with corresponding experimental results.

$$PR = \frac{P_{OJ}}{P_{O\infty}} \tag{1}$$

Once the basic grid and computational strategy was finalized, an effort was made to reduce surface pressure values on the blunt through geometric variations of divergent nozzle jet ejection schemes.

Recent efforts have shown that jet ejected from a cavity can provide better results than jet ejected directly from nose of the body [23]. In this regard, a divergent nozzle was introduced in the nose region of blunt body and the effect of jet ejected from a divergent nozzle was studied. The effect of nozzle geometric variations i.e. divergent angle (θ) and length (L) of nozzle were computed. The nozzle was tested at three divergent angles $\theta = 5°, 10°$ and $15°$. At each angle the nozzle length was varied to 4, 8, 12 and 16 mm. Each geometric case was tested at all three pressure ratios of 0.4, 0.6 and 0.8. Thus a detailed numerical analysis was conducted to reach an optimal configuration under the given flow conditions that would impart minimum drag to the blunt profile under study. **Error! Reference source not found.** is a pictorial summary of the various geometric iterations studied for the divergent nozzle.
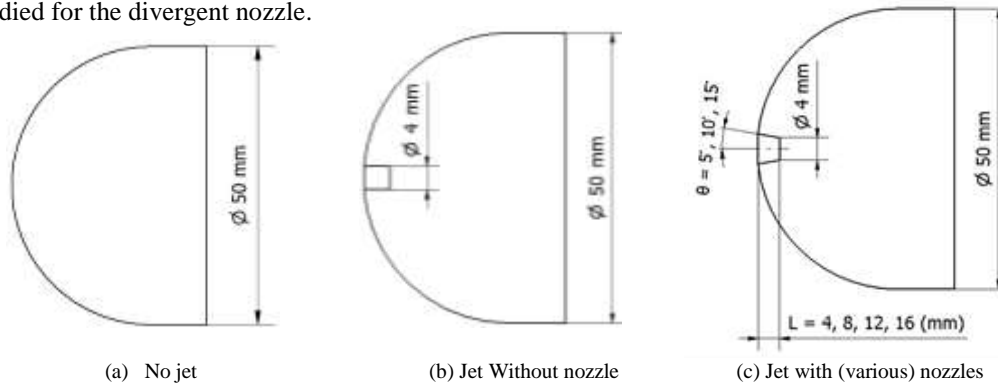

| (a)   No jet | (b) Jet Without nozzle | (c) Jet with (various) nozzles |

Fig. 7   Schematic of various cases studied

3.2.   Numerical Modeling

Precise simulations depend entirely upon the accuracy of formulation of numerical model. Details of numerical modeling and solver settings are provided in the discussion to follow.

3.2.1. Computational Grid and Boundary Conditions

A fully structured 2D axis symmetric computational grid was generated in Gambit®. Due to symmetry of the problem only half of the geometry was modeled. The grid is highly clustered near the body surface and jet orifice in order to accurately resolve complex flow features in these regions. The jet flow boundary was set to pressure inlet. The numerical domain was modeled as far field with outlet modeled as pressure outlet. The selection of these boundary conditions successfully allowed to compute overall mass flow rate of the system and check its conservation. A no slip isothermal condition was applied to the wall. The numerical grid along with the prescribed boundary conditions is shown in Fig 8.
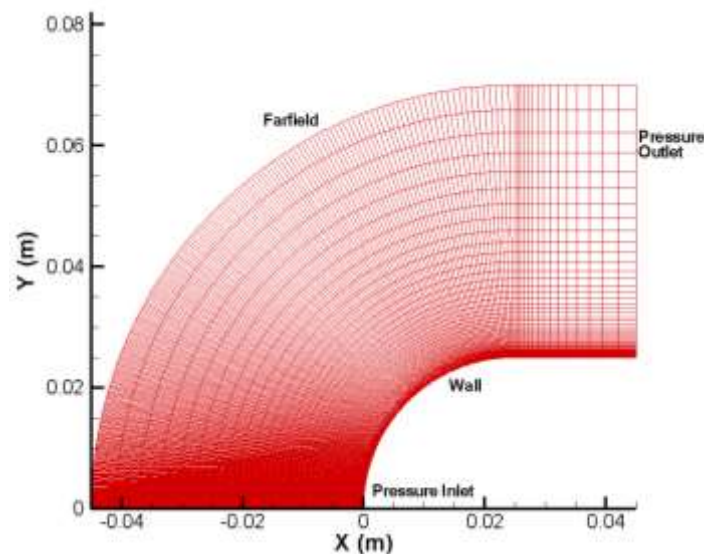

Fig. 8 Numerical Grid with Boundary Conditions

3.2.2. Solver Conditions

The commercially available software ANSYS® FLUENT was used as the numerical solver for all the simulations. Axis symmetric Steady state Reynolds-Averaged Navier-Stokes (RANS) equations were solved using density based implicit solver. Density based formulations solve the governing equations (mass, momentum and energy) simultaneously. Density is the primary variable deduced from mass or continuity equation and pressure is then determined using equation of state. This solver is found to work efficiently in supersonic flows.

The air is modeled as ideal gas as aerothermochemical considerations can be neglected for the current operating conditions. Air viscosity is defined by Sutherland's viscosity law. In order to accurately capture complex flow features such as shockwaves, separation and recirculation regions; a turbulence model was introduced. The K-ω SST turbulence model with default values was used.

4. Results and Discussion

In this work, emphasis is made on alleviation of aerodynamic drag and coupling effects with heating and acoustics considered out of scope of study at this stage. However, it should be noticed that increase in aerodynamic drag, aerodynamic heating and acoustic signature are all positively correlated with surface pressure rise. Reductions in surface pressure implicitly demonstrates no adverse effects on heating and acoustic signatures
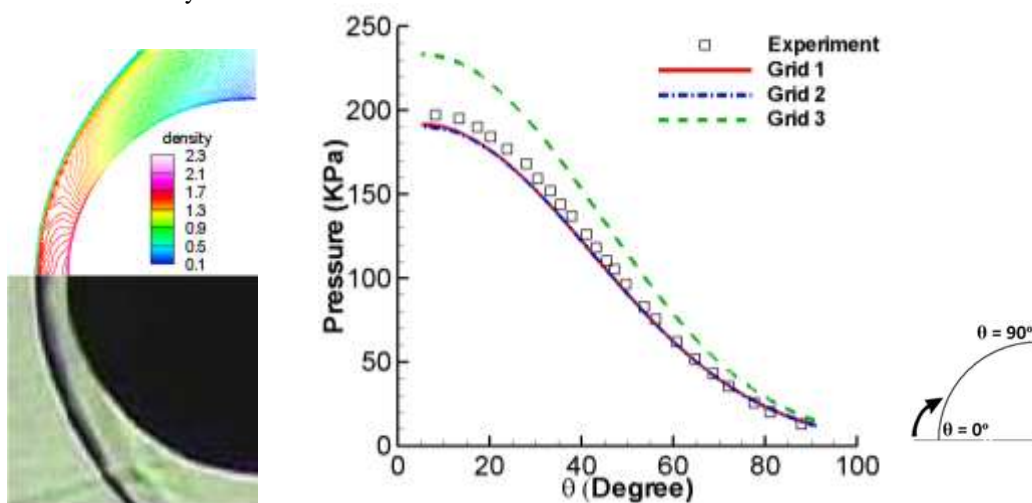
The discussion of results is separated into two sections. The first section discusses the validation cases of simple hemispherical body with and without jet ejection. Surface pressure data are compared with experimental results. Also Mach number and density contours are compared with experimental images. The second section is a detailed discussion on the results obtained by flow visualization as well as geometric variation of divergent nozzle introduced in the forebody region of the hemispherical body.

4.1.   Baseline Validation Cases

4.1.1. Simple Blunt Body (No Jet Case)

The most eminent feature of a blunt body in supersonic flow is formation of a bow shock wave. Other features include a boundary and shock layer. The bow shock is very thin and clearly visible just head of the blunt body. The boundary layer is the region closest to the body with thickness slightly greater than bow shock. The shock layer includes the boundary layer and extends all the way to the bow shock wave. The computed density contours are shown in

9(a). The density contours show that the computed shock stand-off distance is in well agreement with experimental images obtained from the works of Hayashi et al. [27]. A grid independence study was also conducted for the no jet case as shown in **Error! Reference source not found.** 9(b). Three grids; refine grid1 (116000) medium grid2 (67000) and coarse grid3 (45000) were used. The results of the medium grid matched very closely with the fine grid as well as with the experimental surface pressure plots. The medium grid was selected for further analysis.

(a)   Comparison of density contours (kg/m^3)   (b)   Grid independence study of no jet case
       With experimental images

4.1.2. Simple Blunt Body (Jet Injection Cases)

The jet issuing from the nose of blunt body is specified in terms of total pressure ratio P.R. It is the ratio of jet stagnation pressure P_{oj} to free stream stagnation pressure $P_{o\infty}$. Three different pressure ratios tested during experiments were P.R. 0.4, 0.6 and 0.8. Numerical simulations of all three pressure ratios were conducted and duly validated with available surface pressure data. Fig 10 shows surface pressure plots at three pressure ratios. The computed results are found to be in good agreement with the findings of Hayashi et al. [27]. The plot also indicates a decrease in surface pressure with increase in pressure ratio.
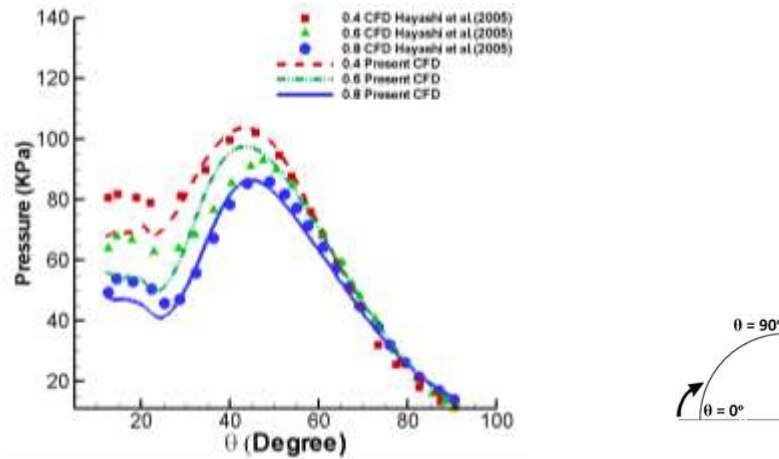

Fig. 10   Surface Pressure Distributions at Various Pressure Ratios

Fig 11 and 12 show computed Mach number contours and density contours compared with experimental images at three pressure ratios respectively. The results indicate that the numerical analysis is successful in capturing all features of jet interaction.
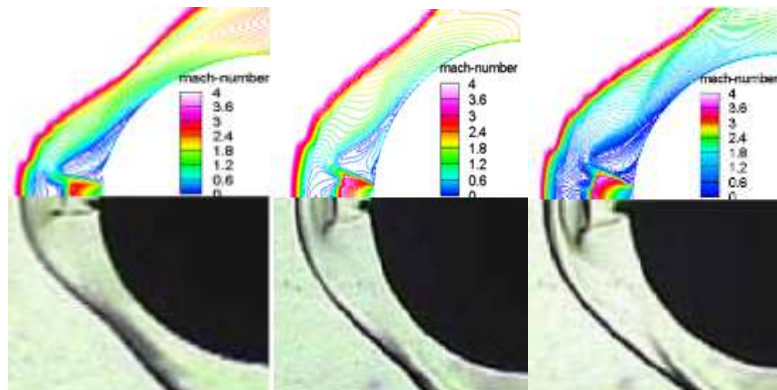

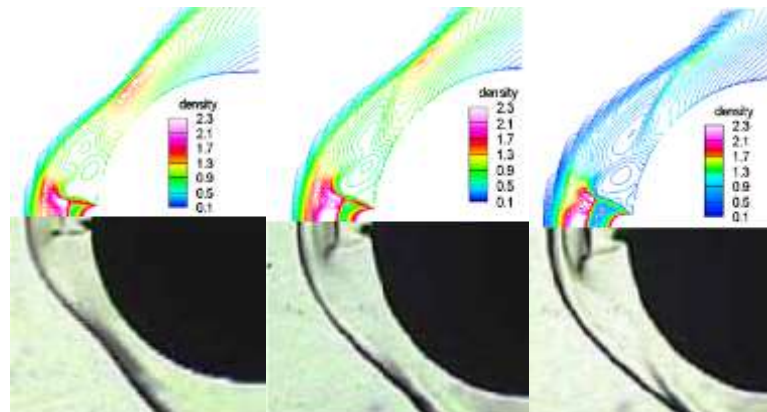Fig. 11   Comparison of mach contours with experimental images [27] for jet cases

9

Fig. 12   Comparison of density contours (*kg/m³*) with experimental images for jet cases

4.2.   Effect of Divergent Nozzle

Once the baseline cases were validated and integrity of the numerical procedure warranted; efforts were made to reduce surface pressure values by introducing a divergent nozzle in the nose region of blunt body. The effect of varying both length and divergent angle of nozzle at different pressure ratios was studied. Both SPM and LPM modes as well as flow separation was observed during various simulations. The theoretical basis discussed earlier provided logical reasoning for the occurrence of these phenomena. The results to follow discuss the effect of geometric variations at each pressure ratio of P.R= 0.4, 0.6, 0.8. The axial Mach number and pressure plots are used to determine whether flow is in LPM or SPM mode. The mach contour images are used to display the flow features of LPM, SPM or flow separation. The surface pressure plots are used to compare the pressure acting on the surface of body under different conditions. The cases exhibiting flow separation are omitted from axial mach and pressure plots as flow separation has three dimensional effects which are not captured accurately by the current two dimensional simulations. Similarly, cases exhibiting LPM are omitted from surface pressure plots as the present steady state simulations cannot capture the transient effects of LPM mode.

For clarity, it is mentioned that all the simulations are assigned a particular notation for example L4 (5). The number following L denotes the length of nozzle and the number in brackets corresponds to nozzle divergent angle. So L4 (5) means a nozzle of length 4 mm and divergent angle of 5°.

4.2.1.   Effect of Geometric Variations at P.R = 0.4

The computed baseline case of simple jet ejected from nose of body at P.R = 0.4 showed SPM. This result was also found in experiments as can be seen from

Fig 11-12. However Hayashi [27] in his findings stated that P.R. = 0.4 was the lower limit at which flow just enters the SPM mode. A well-defined SPM mode was more clearly visible in P.R. = 0.6, 0.8 cases. In the current analysis, only the smallest nozzle case L4 (5) showed SPM, whereas all other length and angular variations showed LPM mode or flow separation inside nozzle for the P.R. of 0.4 cases. The PR of 0.4 cases therefore did not exhibit any favorable results.

Fig 13 shows axial Mach number and pressure variation respectively at different lengths for nozzle of divergent angle θ = 5 °. The axial Mach and pressure plots assist in determining whether flow is SPM or LPM. As shown in

Fig 14, if the axial plot exhibits two distinct shock waves (labeled bow shock and terminal shock in

Fig 14) without a series of weak compression and expansion waves, then it is said to be in SPM. If however, the flow displays a series of compression and expansion waves together with a long shock stand-off distance, then it is said to be in LPM.
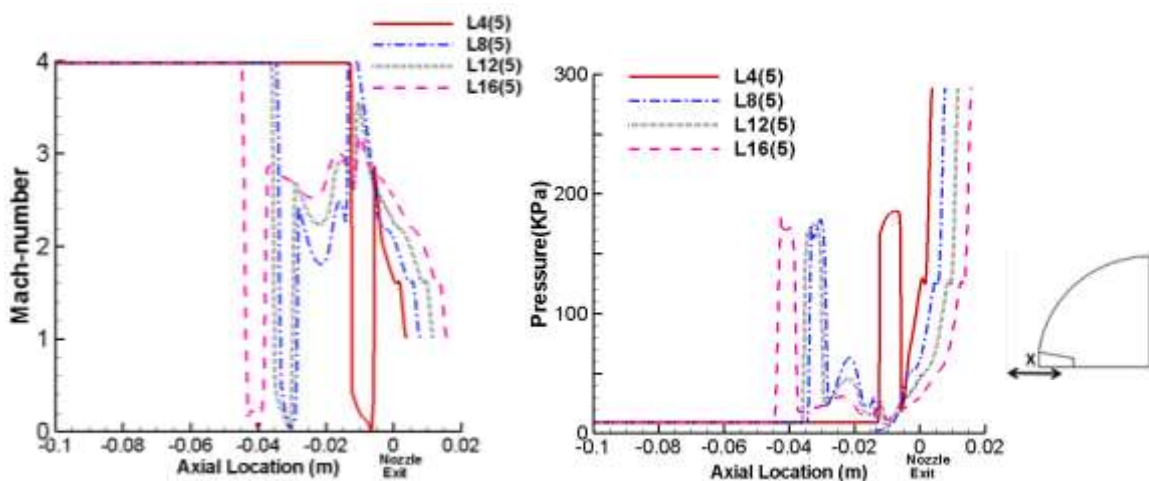

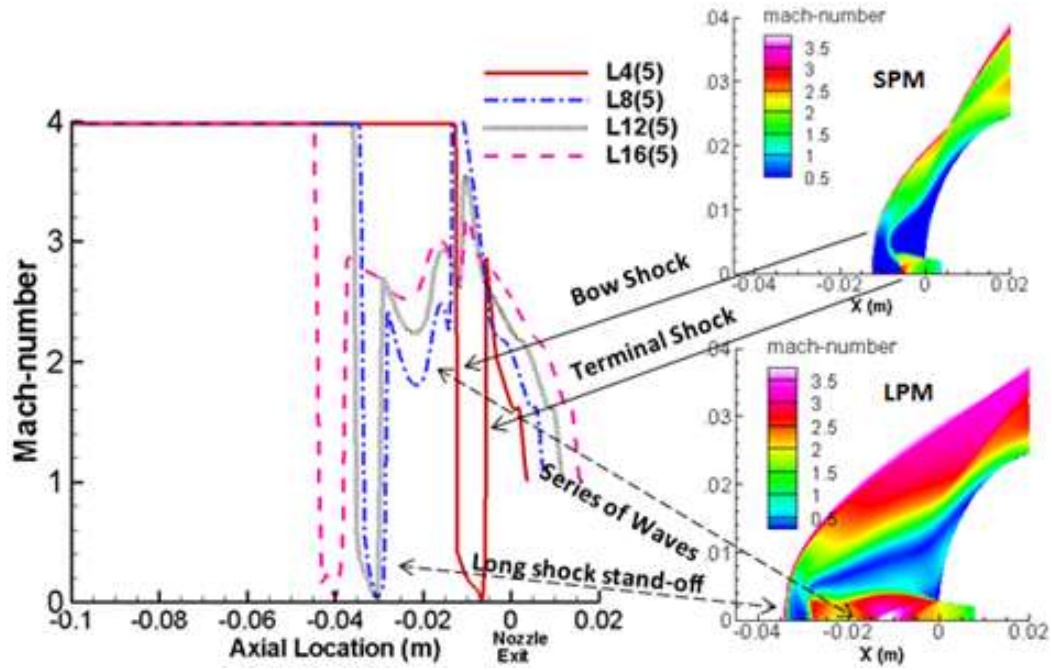Fig. 13   Mach number and pressure distributions along jet axis at different lengths for P.R. = 0.4, θ = 5 °

10

Fig. 14   Identification of Different Flow Modes from Computed Results

Fig 15 shows Mach contour plots at PR = 0.4 for θ = 5 °and 10 ° cases. At each angle the length of the nozzle is varied from 4, 8, 12, 16 mm. Fig 15(a) shows that at P.R. = 0.4 for a small divergent angle θ = 5 °, only the first case L4 (5) shows SPM mode, all other cases show LPM. Fig 15(b) shows mach contour plots at PR = 0.4 for θ = 10 °. The first case L4 (10) shows LPM mode, whereas all other cases show flow separation with in nozzle. The separation becomes more pronounced with increase in nozzle length. Results of θ = 15 ° cases are not presented as they exhibit a similar flow separation scenario.
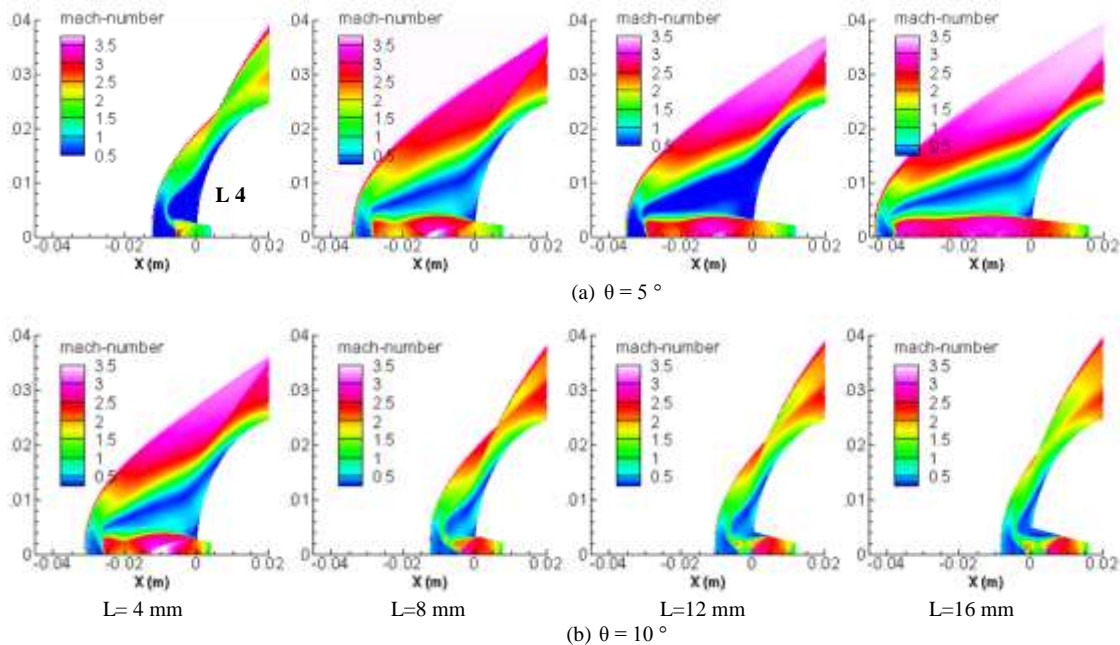

(a) θ = 5 °

L= 4 mm   L=8 mm   L=12 mm   L=16 mm

(b) θ = 10 °

Fig. 15   (a-b) Variation of Mach contour plots at PR = 0.4 with variation in Nozzle Lengths (4, 8, 12, 16 mm) and Angles (θ = 5 ° and 10 °)

The flow separation phenomenon occurs within nozzle due to flow of fluid in reverse direction. For a supersonic divergent nozzle, the static pressure continuously decreases with increasing area. At PR= 0.4, the static pressure of the jet is low. Flow along the nozzle causes further reduction of pressure to such low values that the jet pressure becomes lower than free stream pressure. This causes reverse flow and subsequent flow separation is observed. This is a highly unstable and undesirable phenomenon [28] which generates strong side forces. Flow features no longer remain symmetric and three dimensional effects must be considered. In the

current analysis only contour plots of flow separation are included and corresponding axial pressure or Mach number plots are not presented as they do not include three dimensional effects.

4.2.2. Effect of Geometric Variation at P.R = 0.6

For a small nozzle divergent angle, $\theta = 5°$, increase in nozzle length up to 12 mm showed favorable reduction in surface pressure. However the case L16 (5) at P.R. = 0.6 showed LPM mode. The SPM mode for first three lengths and shift to LPM mode for L16 (5) case can be seen from axial mach and pressure plots of Fig 16.
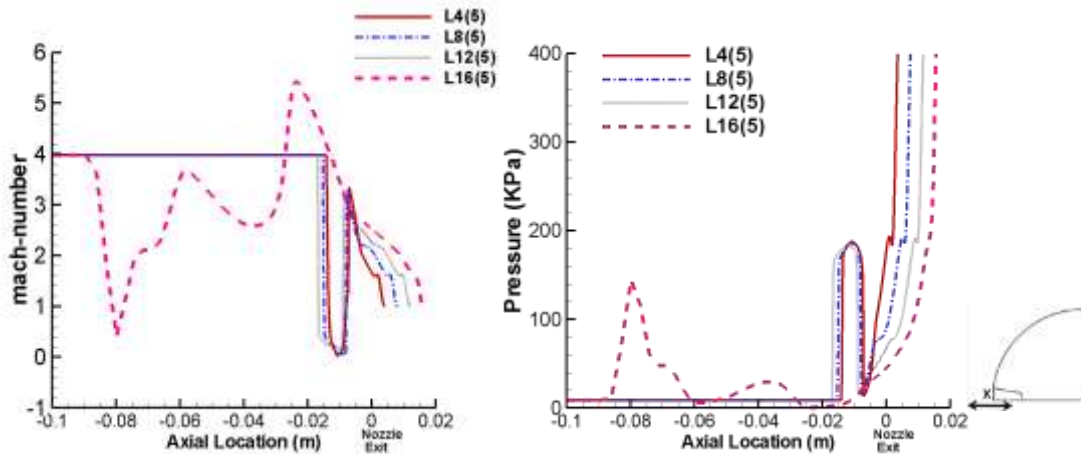

Fig. 16   Mach number and pressure distributions along jet axis at different lengths for P.R. = 0.6, $\theta = 5°$

Fig 17 shows mach contours for the effect of length variation at P.R. = 0.6, for $\theta = 5°$, 10 °and 15 ° cases. It can be seen from Fig(a) that at $\theta = 5°$, flow remains in SPM for the first 3 lengths and then shifts to the LPM for L 16 (5) case. The shift from SPM to LPM is possibly due to the change in jet flow conditions from highly under-expanded to the under expanded jet as mentioned in the literature of section 2. Also the size of recirculation region increases for the first 3 lengths. A greater size of the recirculation region means the flow reattaches further down the fore body region, hence providing a better shielding effect to the blunt body and reducing the surface pressure. Similar results can be deduced from the surface pressure plots of P.R. = 0.6, $\theta = 5°$ case in Fig 18(a). Thus for the P.R. = 0.6, $\theta = 5°$ case increase in length is advantageous only up to L=12mm after which flow becomes unstable.

Fig 17(b) shows mach contours for the effect of length variation at *P.R. = 0.6 and $\theta = 10°$*. The flow remains in SPM for the first 3 lengths after which it exhibits flow separation. The recirculation region remains almost the same for the first two lengths after which it reduces for L 12 (10) case. This behavior can also be observed from the surface pressure plots of Fig 18(b). This means that at higher nozzle divergent angle ($\theta = 10°$) increase in length is advantageous only up to L=8 mm after which it becomes disadvantageous. The last case i.e. L= 16 mm shows flow separation because pressure reduces to such an extent along the divergent nozzle that it causes the jet to become over expanded. Hence flow separation and subsequent shockwaves occur inside the nozzle to reach ambient pressure conditions. A similar trend can be observed for the P.R. = 0.6, $\theta = 15°$ cases in Fig(c). Only the first two lengths are in SPM after which flow separation occurs. There is a marked shrinkage in the recirculation region for the L= 8 mm case. This means only the first case i.e. L4 (15) gives the best results after which there is no further advantage in increasing length. Similar results can be deduced from the surface pressure plots of Fig (c).
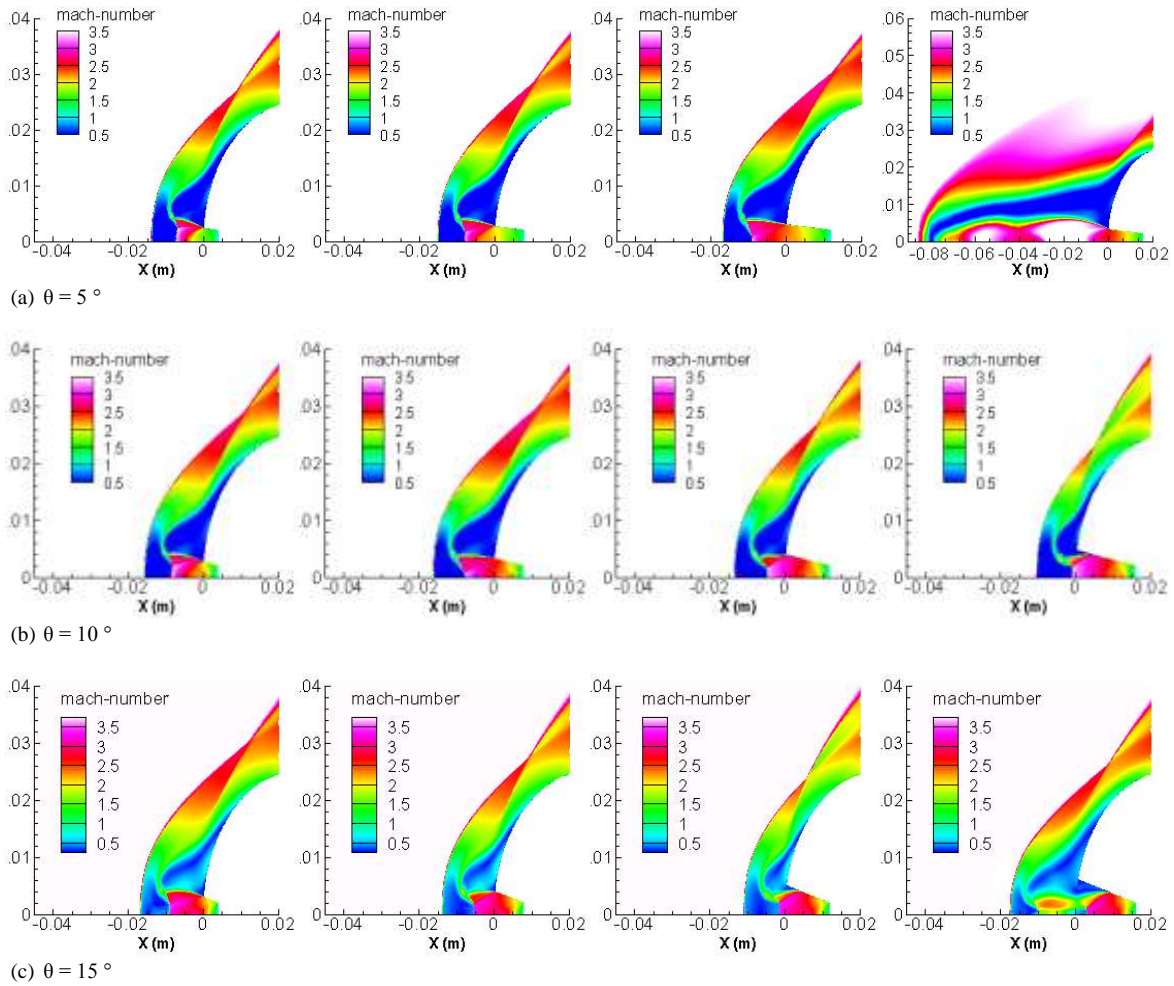
12

(a) θ = 5 °

(b) θ = 10 °

(c) θ = 15 °

Fig. 17 (a-c) Variation of Mach contour plots at PR = 0.6 with variation in Nozzle Lengths (4, 8, 12, 16 mm) and Angles (θ = 5 °, 10 ° and 15°)

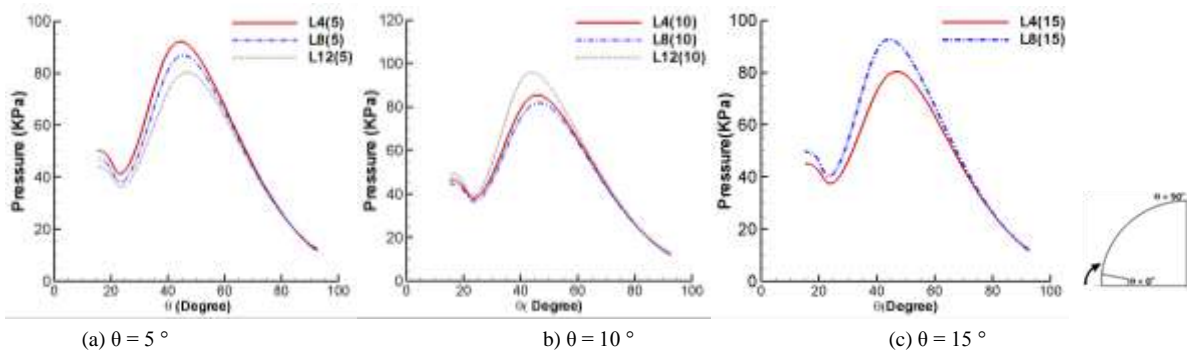(a) θ = 5 °   b) θ = 10 °   (c) θ = 15 °

Fig. 18   Variation in Surface Pressure Distributions with Nozzle Length at PR = 0.6 for θ = 5 °, 10 ° and 15 ° cases.

Fig 18 (a - c) shows surface pressure variations with change in nozzle length at P.R. = 0.6 for the three divergent angles θ= 5 °, 10 °, 15 °. Cases exhibiting LPM or flow separation have been omitted from the plots. From the graphs it can be seen that the cases L12 (5), L8 (10) and L4 (15) give the lowest values of surface pressures.

The Length and angle variations at P.R = 0.6 show that at smaller values of divergent angle; nozzle of greater length is advantageous. However, the reverse is true for higher values of divergent angle, where nozzle of smallest length gives the lowest surface pressure values. To summarize, at P, R = 0.6 three cases L12 (5), L8

(10), and L4 (15) gave the smallest value of surface pressure. Any of these three cases can be selected as the optimal nozzle configuration at P.R = 0.6 based on its advantage in physical implementation.

4.2.3. Effect of Geometric Variation at P.R = 0.8

For small divergent angle θ = 5°, flow remains in SPM mode for all lengths at P.R. = 0.8, this can be seen from axial mach and pressure plots of
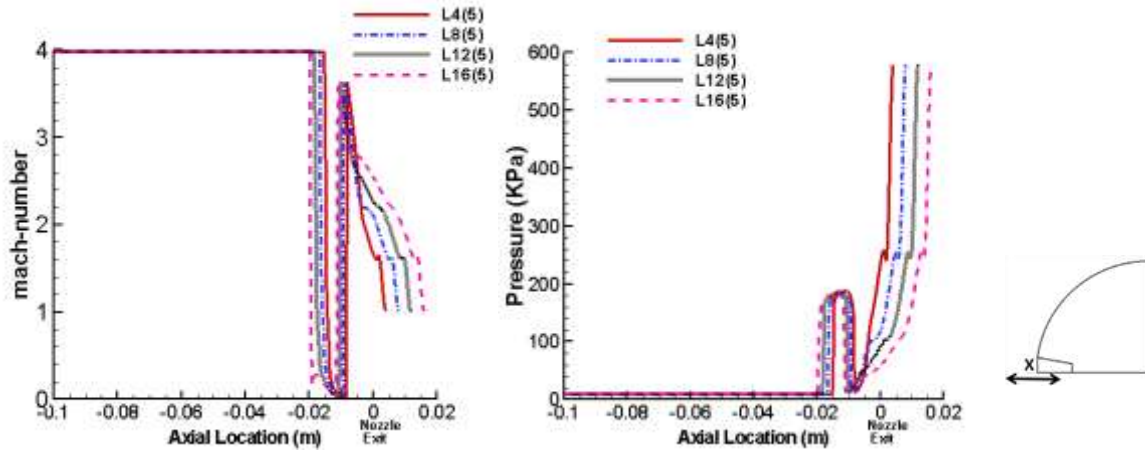Fig 19.

Fig. 19 Mach number and pressure distributions along jet axis at different lengths for P.R. = 0.8, θ = 5 °

For P.R. = 0.8 θ = 5 ° cases, the well-defined SPM flow can be seen from the mach contour images of Fig 20 (a). The recirculation region as well as shock stand-off distance increasing with increase in length from L = 4 to L = 16 mm. The case L16 (5) having the greatest recirculation region and thus giving lowest value of surface pressure as can be seen from surface pressure plots of Fig 21(a). This behavior is similar to that expected from theory. The high P.R of jet causes it to be highly under-expanded at nozzle exit, keeping flow in the stable SPM mode even for the greatest length of 16 mm cases. The greater length of the nozzle at low divergent angles seems to be more advantageous, allowing the flow to fully develop at nozzle exit. Similar to the previous findings, the smallest nozzle divergent angle, θ = 5° gives the best results at largest length L=16 mm.

For θ = 10 °, flow remains in SPM at all lengths Fig 20(b). However, the shock stand-off distance and recirculation region slightly reduce for the L12 (10) case. The reduction becomes more pronounced with increase in length i.e. L 16 (10) case. A similar trend can be noticed in the surface pressure plots of Fig 21(b) where there exists a point of inflexion from L8 (10) to L12 (10) case. The surface pressure decreases up to L8 (10) after which it once again begins to increase with increase in length for the L12 (10) and L16 (10) cases. This means that at higher nozzle divergent angle (θ = 10 °) increase in length is advantageous only up to L=8 mm after which it becomes disadvantageous. Similarly for θ = 15 ° cases only L4 (15) case gives the lowest value of surface pressure. Further increase in length causes an increase in surface pressure until flow separation occurs for the maximum length L = 16 mm case as can be seen from Fig 20(c) and Fig 21(c). Hence at large divergent angle θ = 15° the smallest length case L 4(15) gives the most advantageous results.

(a) θ = 5 °

(b) θ = 10 °
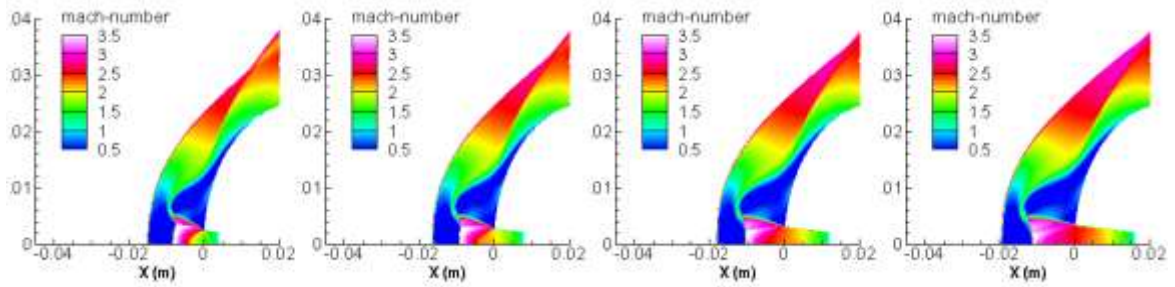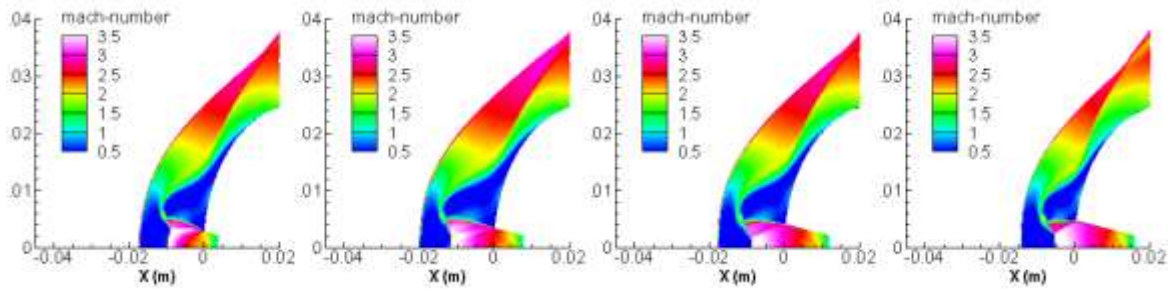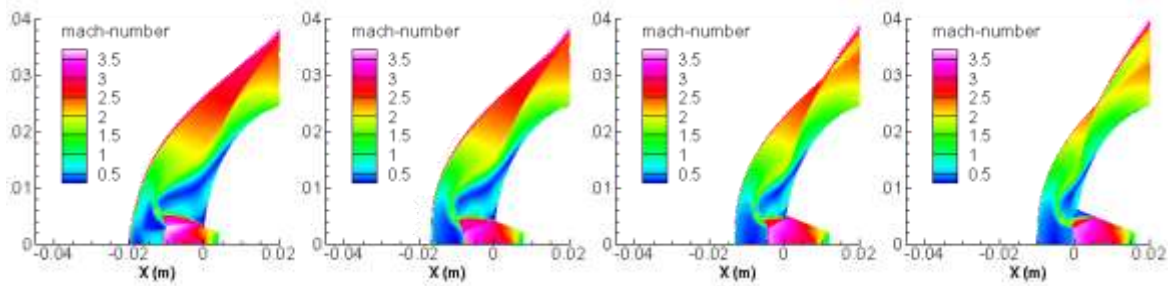
(c) θ = 15 °

Fig. 20 (a-c) Variation of Mach contour plots at PR = 0.8 with variation in Nozzle Lengths (4, 8, 12, 16 mm) and Angles (θ = 5 °, 10 ° and 15°).
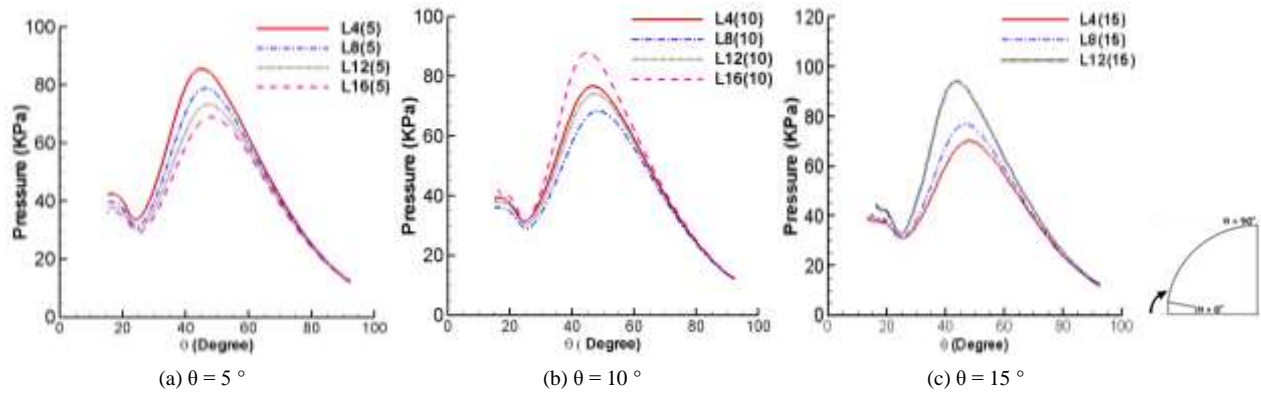
| (a) θ = 5 ° | (b) θ = 10 ° | (c) θ = 15 ° |

Fig. 21   Variation in Surface Pressure Distributions with Nozzle Length at PR = 0.8 for θ = 5 °, 10 ° and 15 ° cases.

Fig 21 (a-c) shows surface pressure variations with change in nozzle length at P.R. = 0.8 for the three divergent angles θ= 5 °, 10 °, 15 °. The linear trend of low surface pressure results with increase in length can be seen in Fig 21(a), this trend continues in Fig 21(b), however the reverse phenomena begins to occur at greater lengths of Fig 20(b) where surface pressure increases with increase in length. This reverse trend follows through to the greater divergent angle θ = 15 ° cases of Fig 21(c). From Fig 21 (a-c) it can be deduced that the cases L 16 (5), L 8 (10) and L4 (15) give the lowest surface pressure values. Any of these three cases can be selected as the optimal nozzle configuration at P.R = 0.8 based on its advantage in physical implementation.

4.3.   Effect of Geometric Variations on Drag Coefficient

The main purpose of the current endeavor was to assess the amount of drag reduction achieved by inserting a divergent nozzle at the nose of a blunt hemispherical body. The surface pressure results of the previous discussion show that a considerable reduction in drag is achieved. In order to compare the drag reduction achieved in each case and gain a better understanding of the effect of various geometric variations, results are summarized in the form of a bar chart in Fig 22. The figure shows the percentage reduction in drag coefficient for each case. The selected baseline case was the simple hemispherical blunt body without any jet. Since the P.R. = 0.4 divergent nozzle cases did not produce any fruitful results hence they are omitted from Fig 21. All cases exhibiting LPM or flow separation are also omitted and only cases displaying the stable SPM flow have been summarized.

From Fig 22 it can be seen that a maximum of approximately 40 % drag reduction can be achieved at P.R = 0.8 without the use of any nozzle. By the use of a divergent nozzle, same reduction can be achieved at a lower pressure ratio of 0.6. A maximum of 46 % [L 4 (15) case] drag reduction can be achieved at P.R = 0.6 with nozzle. Shifting to the P.R = 0.8 nozzle cases a maximum of 56 % drag reduction can be achieved [L8 (10) case].

For each pressure ratio, a general trend can be noticed. At lower divergent angles, the greater nozzle length provides a greater drag reduction. However at higher divergent angles, the reverse phenomenon occurs and greater nozzle lengths provide lesser drag reduction.
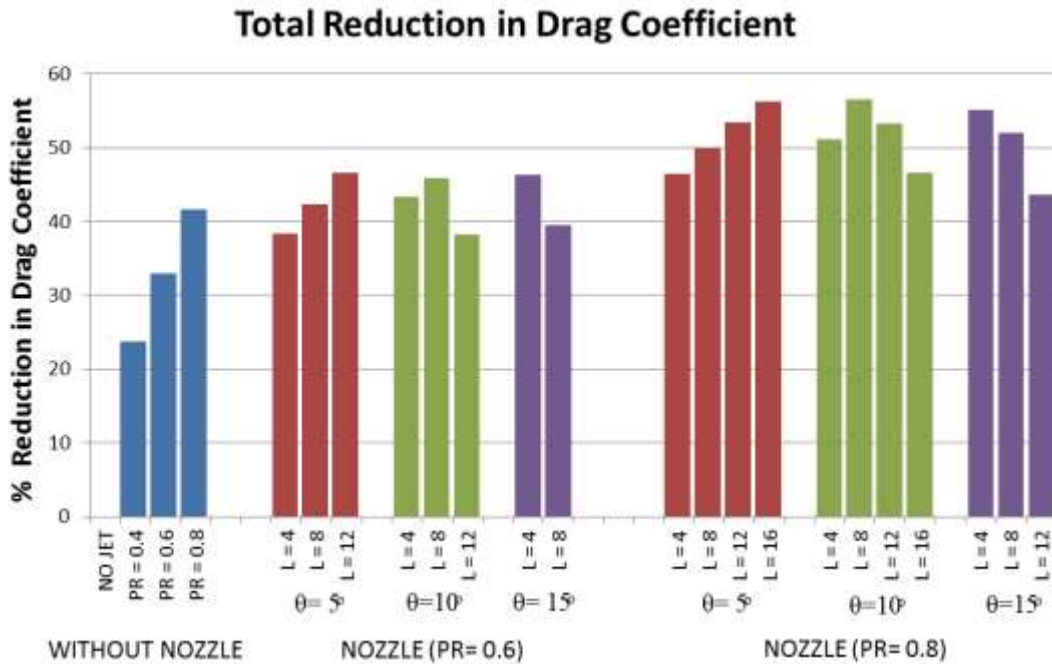
16

Total Reduction in Drag Coefficient

Fig. 22 (%) Reduction in Drag Coefficient

5. Conclusions

The current numerical effort was aimed at understanding the opposing jet concept initially, and ultimately introducing an effective technique for the better application of this newly emerging technology. After numerically validating the baseline experimental cases, a divergent nozzle of varying geometric configurations was introduced at the nose region of the same body. 2d steady state simulations were conducted by varying both length and divergent angle of nozzle at three P.R. = 0.4, 0.6, 0.8 to reach an optimal nozzle and P.R. combination under the given flow conditions. A series of conclusions reached are summarized as follows:

- Without using any nozzle a maximum of approximately 40 % drag reduction can be achieved at P.R = 0.8.

- With a divergent nozzle a better drag reduction can be achieved at a lower pressure ratio 0.6. A maximum of 46 % drag reduction can be achieved [L4(15) case] .

- For P.R = 0.8 nozzle cases, a maximum of 56 % drag reduction can be achieved [L8(10) case].

- For each pressure ratio a general trend can be noticed. At lower divergent angles the greater length provides a greater drag reduction. However at higher divergent angles the reverse phenomenon occurs and greater lengths cause lesser drag reduction.

- The use of a divergent nozzle is therefore recommended as it provides better results at lower pressure ratios.

References

1.   Anderson, J.D., *Fundamentals of Aerodynamics*.
2.   Daso, E.O., et al., *Dynamics of Shock Dispersion and Interactions in Supersonic Freestreams with Counterflowing Jets*. AIAA Journal, 2009. 47(6): p. 1313-1326.
3.   Lopatoff, M., *Wing-Flow Study Of Pressure -Drag Reduction At Transonic Speed By Projecting A Jet Of Air From The Nose Of A Prolate Spheroid Of Fineness Ratio 6*. NACA RESEARCH MEMORANDUM, Oct 1951(RM L51E09).
4.   Love, E.S., *The Effects of a Small Jet of Air Exhausting from theNose of a Body of Revolution in Supersonic Flow*. Nov. 1952. NACA RM L52I19a.
5.   Stadler, J.R. and M. Inouye, *A Method of Reducing Heat Transfer toBlunt Bodies by Air Injection*. May 1956. NACA RM A56B27a.

6. Warren, C.H.E., *An Experimental Investigation of the Effect of Ejectinga Coolant Gas at the Nose of a Bluff Body.* Journal of Fluid Mechanics, 1960. Vol. 8: p. pp. 400–417.
7. Finley, P.J., *The Flow of a Jet from a Body Opposing a Supersonic FreeStream.* Journal of Fluid Mechanics, 1966. Vol. 26: p. pp. 337–368.
8. Rashis, B., *Preliminary Indications of the Cooling Achieved byInjecting Water Upstream from the Stagnation Point of Hemispherical,80_ Conical, and Flat-Faced Nose Shapes at a Stagnation Temperatureof 4000 F.* Oct. 1957. NACA RM L57103.
9. Barber, E.A., *Experimental Investigation of Stagnation PointInjection.* Journal of Spacecraft and Rockets, 1965. Vol. 2(No. 5): p. pp. 770–774.
10. Meyer, B., H.F. Nelson, and D.W. Riggins, *Hypersonic Drag and Heat-Transfer Reduction Using a Forward-Facing Jet.* Journal of Aircraft, 2001. 38(4): p. 680-686.
11. Hayashi, K., S. Aso, and Y. Tani, *Numerical Study on Aerodynamic Heating Reduction by Opposing Jet.* March 2006. Memoirs of the Faculty of Engineering, Kyushu University, Vol.66, No.1.
12. Hayashi, K., S. Aso, and Y. Tani, *Experimental Study on Thermal Protection System by Opposing Jet in Supersonic Flow.* Journal of Spacecraft and Rockets, 2006. 43(1): p. 233-235.
13. Jarvinen, P.O. and R.H. Adams, *The Effects of Retrorockets on the Aerodynamic Characteristics of Conical Aeroshell Planetary Entry Vehicles.* Jan. 1970. AIAA Paper 70-219.
14. Hayashi, K. and S. Aso, *Effect of Pressure Ratio on Aerodynamic Heating Reduction due to Opposing Jet.* 2003.
15. Zheng, Y. and N. Ahmed, *A Novel Means of Dissipation of Shock Wave Induced Heat in a High Speed Flow.* 2013.
16. Nair, P., et al., *Numerical Simulation of Interaction of Sonic Jet with High Speed Flow over a Blunt Body using Solution Mapped Higher Order Accurate AUSM+-UP Based Flow Solver.* Journal of Applied Fluid Mechanics, 2010. Vol. 3, No. 1: p. pp. 15-23.
17. Shah, B.H. and X.-Y. Lu, *Computational Study of Drag Reduction at Various Freestream Flows Using a Counterflow Jet from a Hemispherical Cylinder.* Engineering Applications of Computational Fluid Mechanics, 2014. 4(1): p. 150-163.
18. Jarvinen, P. and R.H. Adams, *The Aerodynamic Characteristics Of Large Angled Cones With Retrorockets.* Feb 1970. NASA 7 - 576.
19. Korzun, A., J.C. Cordell, and R. Braun, *Comparison of Inviscid and Viscous Aerodynamic Predictions of Supersonic Retropropulsion Flowfields.* 2010.
20. Sriram, R. and G. Jagadeesh, *Film Cooling at Hypersonic Mach Numbers using Forward Facing Array of Micro-jets.* International Journal of Heat and Mass Transfer, 2009. 52(15-16): p. 3654-3664.
21. Tamada, I., S. Aso, and Y. Tani, *Reducing Aerodynamic Heating by the Opposing Jet in Supersonic and Hypersonic Flows.* 2010. AIAA.
22. Morimoto, N., et al., *Reduction of Aerodynamic Heating with Opposing Jet through Extended Nozzle in High Enthalpy Flow.* AIAA 2014.
23. Lu, H. and W. Liu, *Investigation of Thermal Protection System by Forward-Facing Cavity and Opposing Jet Combinatorial Configuration.* Chinese Journal of Aeronautics, 2013. 26(2): p. 287-293.
24. Huang, W., et al., *Drag and Heat Reduction Mechanism in the Combinational Opposing Jet and Acoustic Cavity Concept for Hypersonic Vehicles.* Aerospace Science and Technology, 2015. 42: p. 407-414.
25. http://www.aerospaceweb.org/question/propulsion/q0220.shtml.
26. http://www.allstar.fiu.edu/aero/rocket3.htm.
27. Hayashi, K., S. Aso, and Y. Tani, *Numerical Study of Thermal Protection System by Opposing Jet.* 2005.
28. Abdellah Hadjadj, M.O., *Nozzle flow separation.* Springer 2009. Shock Waves (2009) 19: p. 163–169.